Anomalous *P-E* Hysteresis Loops of Ferroelectric Nanocomposites Containing Nanocellulose and Hydrogen – Bonded Ferroelectric of Triglycine Sulfate Under Influence of Composition, Temperature and Moisture

Hoai Thuong NGUYEN *

Faculty of Electrical Engineering Technology, Industrial University of Ho Chi Minh City, Nguyen Van Bao 12, 700000, Ho Chi Minh City, Vietnam

crossref http://dx.doi.org/10.5755/j02.ms.30250

Received 05 December 2021; accepted 13 January 2022

To fill the gap of earlier works for the nanocomposite based on a ferroelectric of triglycine sulfate (TGS) and a dielectric inclusion of cellulose nanoparticles (CNP), the present study provides experimental results for investigating anomalous switching properties via analyzing the features of dielectric (*P-E*) hysteresis loops. Different dielectric content of CNP (5, 15, 30, 50, 70 wt.%) was chosen. The *P-E* loops were measured at temperatures placed at the same distances from the phase transition point for all compositions. Besides, the influence of humidity (RH = 30, 60, 80, 100 %) was also investigated. It was clarified that the increase in cellulose content and relative humidity caused the increase in coercive field, accompanying the transformation of hysteresis loops from saturated into unsaturated ones. The nature of these anomalies was proposed to be associated with the role of hydrogen bonds in the composite.
Keywords: P-E hysteresis loops, ferroelectrics, triglycine sulfate, phase transition, nanocellulose.

1. INTRODUCTION

The improvement of technology cannot be separated from the modernization of materials which help to bring the ideas from a fundamental level to everyday life through devices that are made of materials [1 – 3]. Luckily, up to now, materials science has still been capable of catching up with technology growing. In this context, ferroelectrics have always been being a promising candidate [4, 5].

Hydrogen-bonded ferroelectrics (HBF) are multifunctional materials possessing ferroelectricity created by the behavior of hydrogen bonds in their structures. This kind of ferroelectrics is well known with two candidates of triglycine sulfate (TGS) and Rochelle salt (RS) that can be found in UV tunable laser, pyroelectric infrared sensors [6, 7] oscillators and transducers [8, 9]. Due to the run-out-of interest in the primary HBF ferroelectrics, researchers have switched the lens to HBF-based nanocomposites, the properties of which can be controlled by hydrogen-containing inclusions [7, 9 – 12]. In previous studies [7, 13], our research team has developed an HBF-based nanocomposite from cellulose nanoparticles (CNP) combined with TGS. The works reported experimental results for phase transition and relaxation properties. It was clarified that the hydrogen bonds between CNP and TGS components for both dried and wet samples dragged the Curie point toward higher temperatures. The effect became stronger with increasing the inclusion content and relative humidity. Besides, due to the increased viscosity at the inclusion/ferroelectric interfaces, the domain-wall motions were restricted and led to the reduction of relaxation frequencies [13]. It is worth noting that cellulose nanoparticles have a huge advantage over the common nanofibers because the ferroelectric inclusion content can be easily adjusted.

Despite the fact that the phase transition and relaxation properties are indispensable for applications of ferroelectric materials in electronics, the above results are not enough and therefore further research is needed. Particularly, materials used for the fabrication of nonvolatile ferroelectric random-access memories must possess good switching characteristics. However, in the mentioned works, the switching properties involving the reversal of polarization have not been considered yet. Moreover, along with practical potential, exploring the switching properties of ferroelectric composites is essential to improve the fundamental knowledge in the field of materials science.

In this regard, to fill the shortcomings of earlier works, the present study provides experimental results for clarifying anomalies of *P-E* hysteresis loops for CNP+TGS samples under the influence of composition, temperature and moisture.

2. EXPERIMENTAL METHODS

The synthesis procedure of the CNP+TGS composite has been described in detail in previous studies [7, 13]. The authors herein carefully characterized the samples of composite as well as starting materials. The utilized crystalized CNP was determined as 40 – 80 nm in size [13]. The preparation process can be summarized as follows. Firstly, a saturated ferroelectric solution of TGS was prepared at room temperature (25 °C). Meanwhile, CNP must be stored in the water right after obtaining from cotton [14]. Otherwise, cellulose nanoparticles could be stuck together in the dried form and were not easy to separate in

* Corresponding author. Tel.: +84868844310.
E-mail address: *nguyenthuongfee@iuh.edu.vn* (H. T. Nguyen)

water again. In the present work, we picked CNP with 5, 15, 30, 50, 70 % of total sample weight to combine with TGS to test the effects of composition on switching properties. To estimate the composition weight ratio, a determined volume of each "aqueous" CNP was taken out and dried for weighing before preparation. The mixture of CNP+TGS for each composition was initially stirred in a closed bottle, then in the open air to get a viscous form. The obtained one was left in the open air for a few days, then dried to remove residual water. However, residual water cannot be removed completely from composite samples because it could be absorbed again under the normal conditions. The presence of water was also confirmed by Fourier-transform infrared spectroscopy in the previous study [13]. For investigation of the influence of humidity on switching properties, the composite samples were kept under different relative humidity (RH) of 30, 60, 80 and 100 % for 3 days at room temperature.

The dielectric hysteresis loops were taken at 1 kHz on a Precision LC tester (Radiant Technology, Korea) at temperatures placed at different distances from the phase transition point for each composition. The GW Instek LCR-821 meter was utilized to determine the phase transition temperatures in the synthesized composite samples at 1 kHz. The measurement error did not exceed 1 %.

3. EXPERIMENTAL RESULTS AND DISCUSSION

3.1. Reliability of samples

The reliability of samples of CNP+TGS composite and starting materials has been confirmed in previous studies using XRD and FTIR techniques [7, 13]. Let us review some main features that could be useful in the present study.

For XRD patterns, the presence of CNP did not cause the movement of peak positions i.e. the crystalline structures of composite components remained unchanged, even though the peaks of CNP became more pronounced and of TGS – less pronounced when adding CNP [7, 13]. Under the influence of relative humidity (RH) up to 100 %, the significant adjustment of XRD was not detected, except for changes in intensities.

In the case of FTIR patterns, the situation is more complicated. In the composite state, the possible formation of new hydrogen bonds between CNP and TGS, as well as the increase in OH^- groups with increasing CNP led to the expansion of adsorption peaks at wavenumbers higher 2800 cm^{-1} [7]. Under higher relative humidity, the same anomaly was also observed [13]. Besides, the peaks for groups of SO_4^{2-}, which are characteristic for ferroelectricity in TGS, were shifted toward a lower wavelength with increasing RH.

3.2. Phase transition in CNP+TGS composite

The changes of phase transition point T_c under the influence of CNP content and humidity are presented in Fig. 1 and Table 1. Although the influence of humidity on the phase transition of the composite was reported in our previous study [13], the effect of composition has not been considered yet. Seeing that the addition of CNP dragged T_c toward higher temperatures (Fig. 1). This anomaly was related to the interaction between CNP and TGS through hydrogen bonds [13], the strength of which could be amplified with more cellulose nanoparticles surrounding TGS crystals at high CNP content. The effects of humidity were more interesting. The higher the relative humidity was, the higher the T_c could be detected (Fig. 1). However, this was insignificant at relatively low CNP content or high T_c (T_c > 90 °C) (Fig. 1). The reason might be associated with the fact that composite samples with small CNP content absorbed very little water which could be quickly removed from the sample surface in the heating process. In the case of high T_c, we supposed that the residual water molecules had been vaporized before reaching the phase transition point. According to our recording, the strongest influence of humidity on phase transition was detected for composite samples with a CNP of 30 wt.% (Fig. 1).

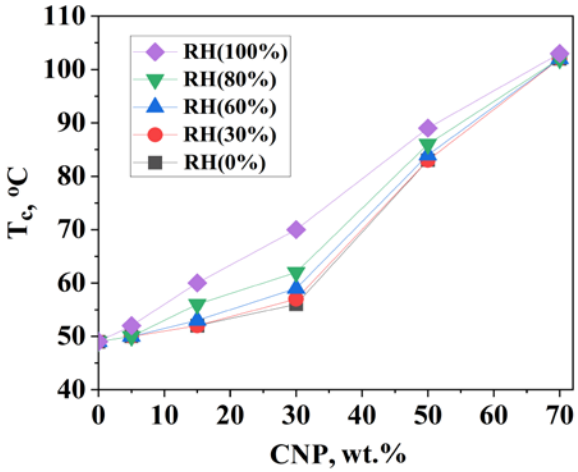

Fig. 1. Dependences of phase transition temperatures T_c on CNP content under different relative humidity

Table 1. Phase transition in CNP+TGS composite at different CNP content and relative humidity (RH)

RH, %	Tc, °C					
	Pure TGS	CNP (5 wt.%)	CNP (15 wt.%)	CNP (30 wt.%)	CNP (50 wt.%)	CNP (70 wt.%)
Dried samples	49	50.1	52.2	55.8*	83.1*	102.1*
30	49	50.2	52.4	56.9	83.3	102.2
60	49	50.1	53.1	58.8	84.2	101.7
80	49	50.3	55.9	62.3	85.8	101.5
100	49	52.2	60.2	69.7	88.6	103.3
* These values have been obtained in the previous work [13]						

3.3. Switching properties

The reliability of pure TGS has been also confirmed by the *P-E* hysteresis loops shown in Fig. 2 at temperatures *T* placed at different distances (ΔT = -25, -10, -5, -1 °C) from Curie point (T_c = 49 °C), where $\Delta T = T - T_c$. The minus values of ΔT as noted in Fig. 2 mean for a ferroelectric phase in which the measurements took place. The saturation polarization P_s, residual polarization P_r and coercive field E_c are listed in Table 2. Obviously, the *P-E* loops have the characteristic form for TGS with P_s, P_r and E_c values in good consistent with those reported in the literature [15]. Besides, the heating charge led to the decrease in P_s P_r and E_c (Fig. 2, Table 2) due to the gradual increase in symmetry and the release of domains from possible defects when reaching the phase transition point [16].

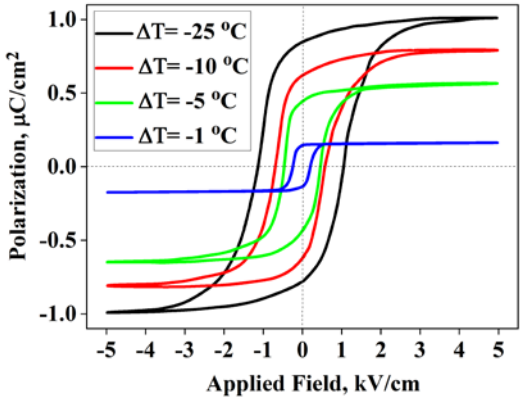

Fig. 2. *P-E* hysteresis loops for pure polycrystalline TGS at different distances from Curie point T_c = 49 °C

Table 2. The values of saturation polarization P_s and coercive field E_c of pure TGS at different distances ΔT from its Curie point T_c = 49 °C

ΔT, °C	P_s, μC/cm²	P_r, μC/cm²	E_c, kV/cm
-25	1.01	0.85	1.13
-10	0.79	0.63	0.67
-5	0.56	0.45	0.45
-1	0.17	0.15	0.24

When adding the dielectric inclusion of CNP into TGS, the saturated *P-E* loops were also detected with CNP content less than about 50 wt.% (Fig. 3). The loops tended to transform from saturated shapes to ellipses with increasing CNP. Perhaps, the ellipses will be transformed back to the saturated loops at higher applied fields. Unfortunately, we have failed to obtain them because the samples have been broken down before reaching saturation. However, the saturated curves could be obtained at higher CNP content in the vicinity of the phase transition point (Fig. 4). Regarding the loop parameters, we considered the dependences of maximum polarization P_{max} (Fig. 5 a), residual polarization P_r and coercive field E_c (Fig. 5 b) on CNP content and temperature. Noted that $P_{max} = P_s$ in the case of saturated loops. Interestingly, the increase in CNP percentage caused the reduction of P_{max} (Fig. 5 a), P_r (Fig. 5 b) and the rise in E_c (Fig. 5 c). Moreover, in the vicinity of phase transition (ΔT = -1 °C), the changing rate of these values with CNP content was insignificant (Fig. 5). It should be noted that the bias field was small, and the loops were quite symmetric. All the mentioned anomalies will be discussed thoroughly in this study.

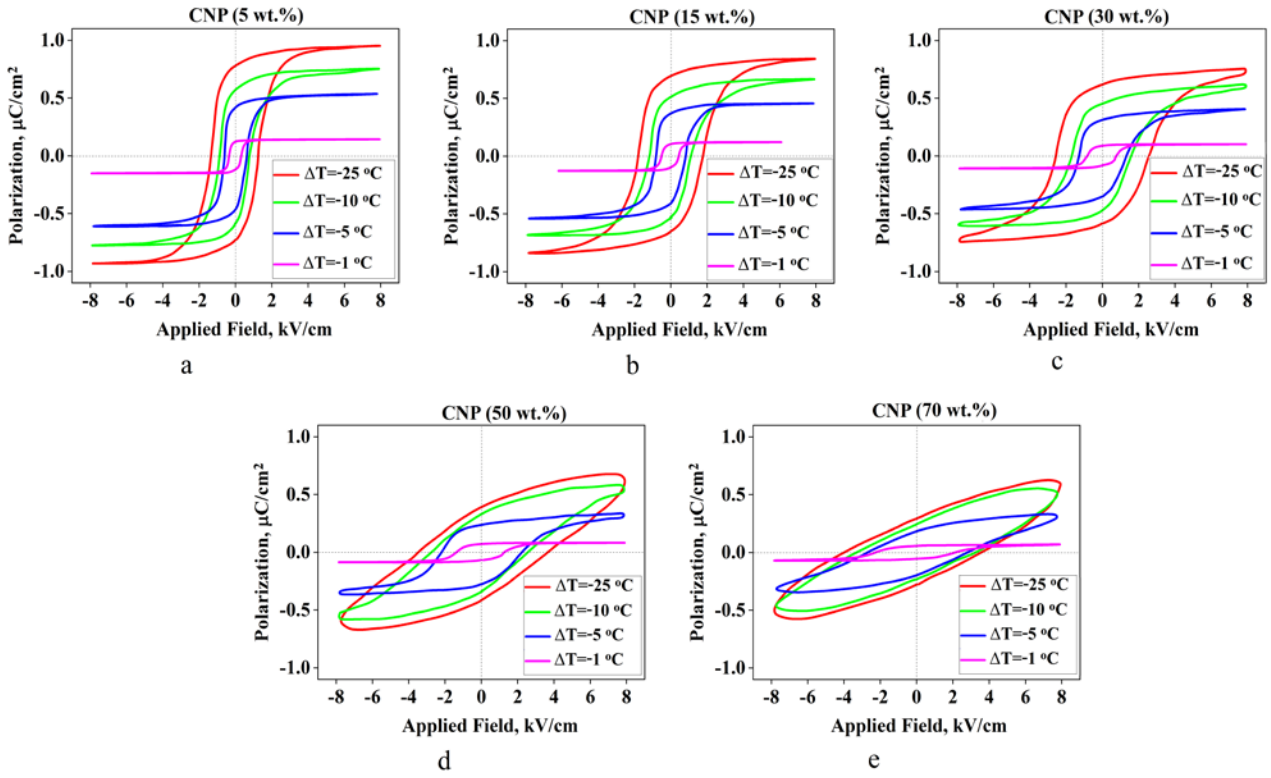

Fig. 3. *P-E* hysteresis loops placed at different distances from phase transition point for dried composite samples containing different CNP contents: a – 5 wt.%; b – 15 wt.%; c – 30 wt.%; d – 50 wt.%; e – 70 wt.%. The measuring electric field of 8 kV/cm was applied for all samples

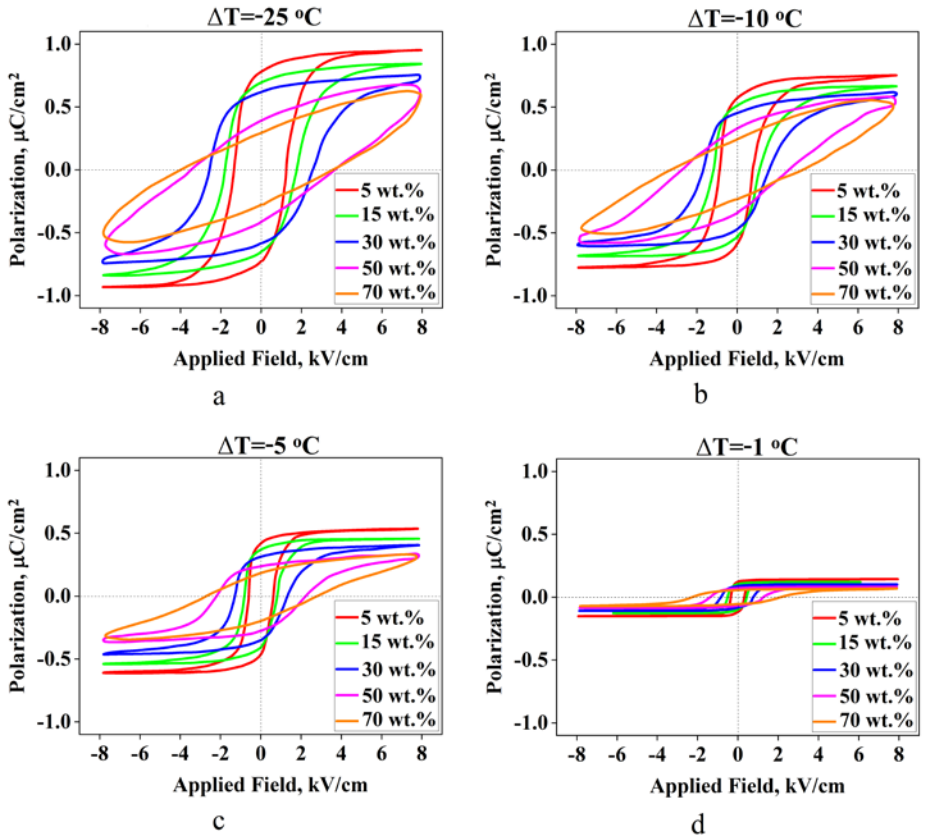

Fig. 4. *P-E* hysteresis loops of dried composite samples containing different CNP contents for temperatures placed at different distances from phase transition point of *ΔT*: a – -25 °C; b – -10 °C; c – -5 °C; d – -1 °C. The measuring electric field was 8 kV/cm for all samples

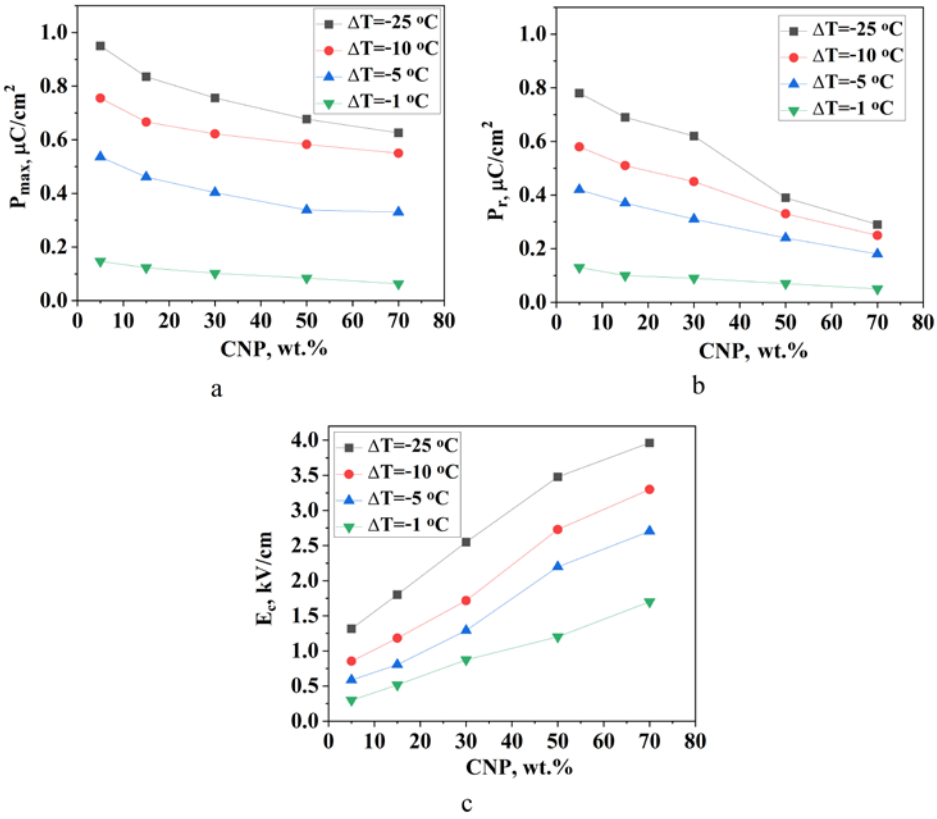

Fig. 5. a – dependences of maximum polarization; b – coercive field on CNP content at different temperatures from phase transition points

The dielectric hysteresis loops for the composite samples stored under different RH at room temperature are shown in Fig. 6. The samples with a CNP of 30 wt.% were chosen because of giving the most significant influence as indicated in Fig. 1. Observing that the higher the relative humidity, the higher the values of residual polarization and coercive field. The shape of *P-E* loops was deformed from saturated curves and gradually turned into the ones that are characteristic of those with current leakage. For other CNP content, a similar behavior has been also observed, but with a less obvious effect.

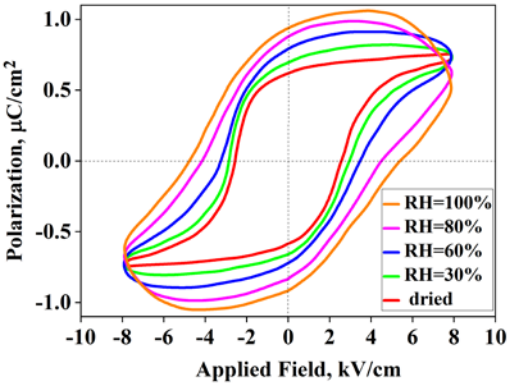

Fig. 6. *P-E* hysteresis loops for wet composite samples (CNP 30 wt.%) under different RH at ΔT = -25 °C

3.4. Discussion

As mentioned above, the presence of CNP in TGS led to several anomalies for dielectric hysteresis loops that could be adjusted during the heating process. We will point-by-point analyze these anomalies.

Firstly, the transformation of *P-E* loops from saturated to ellipse shapes with increasing CNP content was probably related to the restricted state of domain-wall (DW) motion in TGS crystals due to the interaction between CNP and TGS through hydrogen bonds [7]. Indeed, the domain sideway displacement X of TGS can be found according to the following equation [17]:

$$kX + \eta\ddot{X} = 2P_sE, \quad (1)$$

where k, η are elastic and viscous parameters, respectively; P_s is the spontaneous polarization; E is the applied field. Based on the type of differential Eq. 1, the polarization switching is hindered with increasing viscosity η [18]. Moreover, the increased viscosity related to the hydrogen bonds between CNP and TGS [13] could be responsible for the reduction of maximum and residual polarization, as well as for the rise in a coercive field with increasing cellulose percentage (Fig. 5).

Secondly, the decrease in P_{max}, P_r and E_c with shortening the distances from measuring temperature to phase transition point (Fig. 5) can be understood based on the knowledge of ferroelectric materials. In this case, the heating charge in the ferroelectric phase helps to release domains from possible defects, leading to the reduction of E_c. However, along with this process, the asymmetry will be gradually lowered ($P_s \rightarrow 0$) and completely disappear at the phase transition point ($P_s = 0$). This can also explain why at high CNP content, the saturated P-E loops were obtained in the vicinity of phase transition. In some ferroelectric materials, the dependences of P_s on distances ΔT from measuring temperature to phase transition point can be expressed as $P_s \sim 1/\Delta T$ [19].

Thirdly, in the vicinity of phase transition, the changes of P_s, P_r and E_c were insignificant at high CNP content (Fig. 5). As clarified above, the structure of TGS gradually transformed into a symmetric one. In addition, the samples with high CNP content have higher phase transition temperatures and therefore the influence of hydrogen bonds formed between CNP and TGS was weaker.

The deformed shapes of *P-E* loops obtained for wet samples were related to the presence of current leakage [20, 21] due to the absorbed water that allows charge carriers to move easier. These charge carriers might be originated from possible impurities that could not be avoided in materials. Luckily, they did not bring effects on ferroelectricity for dried samples as described above. Besides, the increase in the coercive field and residual polarization might be associated with the hydrogen bonds formed in the wet composite. Indeed, these bonds could stabilize the polar state of TGS at higher temperatures i.e. the phase transition temperatures increased (Fig. 1).

The detected small bias field could be related to the even distribution of CNP and TGS inside the composite samples.

4. CONCLUSIONS

Based on the above analysis, several anomalous switching properties under influence of composition, temperature and humidity for the composite consisting of cellulose nanoparticles and TGS polycrystals have been figured out. The increase in cellulose content as well as relative humidity, led to the transformation of the loops from saturated into unsaturated ones along with the increase in the coercive field due to amplifying the role of hydrogen bonds that inhibit the motion of domain walls in TGS. Regarding the effects of measuring temperature, the saturated hysteresis loops were easier to obtain when reaching phase transition temperatures because of the release of domain walls from possible defects as always observed in ferroelectrics. The research suggests a promising way to design ferroelectric materials with the required properties.

REFERENCES

1. **Daoush, W. M.** Strength of Materials: Fundamentals and Applications (First Edition). Cambridge University Press, 2018: 672 p. https://doi.org/10.1557/mrs.2020.322
2. **Suhana, M. S., Mohd, F.M.S., Faiz, S., Mohamad, R.** Ferroelectrics and Their Applications, Encyclopedia of Smart Materials, Elsevier, 2022: pp. 495 – 506. https://doi.org/10.1016/B978-0-12-815732-9.00105-4
3. **Neil, D.M.** Magnetic Materials: Fundamentals and Device Applications *Physics Today* 56 (12) 2003: pp. 62 – 64. https://doi.org/10.1063/1.1650232
4. **Mikolajick, T., Slesazeck, S., Mulaosmanovic, H., Park, M.H., Fichtner, S., Lomenzo, P.D., Hoffmann, M., Schroeder, U.** Next Generation Ferroelectric Materials for

Semiconductor Process Integration and Their Applications *Journal of Applied Physics* 129 (10) 2021: pp. 100901. https://doi.org/10.1063/5.0037617

5. **Anisimovas, F., Ašmontas, S., Kiprijanovič, O., Maneikis, A., Vengalis, B.** Broadband Electromagnetic Emission from PZT Ferroelectric Ceramics after Shock Loading *Materials Science (Medžiagotyra)* 19 (4) 2013: pp. 433 – 437. https://doi.org/10.5755/j01.ms.19.4.3137
6. **Farhana, K., Jiban, P.** Synthesis, Growth, and Electrical Transport Properties of Pure and $LiSO_4$ -Doped Triglycine Sulphate Crystal *International Journal of Optics* 2012 (803797) 2012: pp. 1 – 6. https://doi.org/10.1155/2012/803797
7. **Mai, B.D., Nguyen, H.T.** Influence of Gamma Irradiation on Properties of Ferroelectric Composite from Cellulose Nanoparticles and Triglycine Sulfate *Materials Transactions* 60 (9) 2019: pp. 1902 – 1907. https://doi.org/10.2320/matertrans.MT-M2019139
8. **Mathivanan, V., Haris, M., Chandrasekaran, J.** Thermal, Magnetic, Dielectric and Anti Microbial Properties of Solution-Grown Pure and Doped Sodium Potassium Tartrate Crystals *Optik* 127 (4) 2016: pp. 1804 – 1808. https://doi.org/10.1016/j.ijleo.2015.11.092
9. **Mai, B.D., Nguyen, H.T., Hoang, D.Q.** Influence of Cellulose Nanoparticles on Structure and Electrophysical Properties of Ferroelectrics *Materials Transactions* 60 (12) 2019: pp. 2499 – 2505. https://doi.org/10.2320/matertrans.MT-M2019189
10. **Mai, B.D., Nguyen, H.T., Hoang, D.Q.** A Novel Composite from Nanodispersed Silica and an Organic Ferroelectric of Diisopropylammonium Bromide: Preparation, Characterization and Dielectric Properties *Materials Transactions* 60 (10) 2019: pp. 2132 – 2136. https://doi.org/10.2320/matertrans.MT-M2019157
11. **Nguyen, H.T., Chau, M.T., Nguyen, V.A.** Anomalous Dielectric Properties of Ammonium Sulfate Under Nanoconfinement in a Natural Matrix of Cellulose *Phase Transitions* 93 (10 – 11) 2020: pp. 1048 – 1054. https://doi.org/10.1080/01411594.2020.1832223
12. **Nguen, K.T., Milovidova, S.D., Sidorkin, A.S., Rogazinskaya, O.V.** Dielectric Properties of Composites Based on Nanocrystalline Cellulose with Triglycine Sulfate *Physics of the Solid State* 57 2015: pp. 503 – 506. https://doi.org/10.1134/S1063783415030178
13. **Mai, B.D., Nguyen, H.T., Ta, D.H.** Effects of Moisture on Structure and Electrophysical Properties of a Ferroelectric Composite from Nanoparticles of Cellulose and Triglycine Sulfate *Brazilian Journal of Physics* 49 2019: pp. 333 – 340. https://doi.org/10.1007/s13538-019-00658-5
14. **Tayebeh, F.M., Fatemeh, D., Gity, M.M.S., Hamid, E.Z.A.** Spherical Cellulose Nanoparticles Preparation from Waste Cotton Using a Green Method *Powder Technology* 261 2014: pp. 232 – 240. https://doi.org/10.1016/j.powtec.2014.04.039
15. **Albert, S., Robert, C.M.** Asymmetric Hysteresis Loops and the Pyroelectric Effect in Triglycine Sulfate *Journal of Applied Physics* 30 (11) 1959: pp. 1646 – 1648. https://doi.org/10.1063/1.1735028
16. **Karin, M., Rabe Charles, H., Ahn, J.M.T.** Physics of Ferroelectrics (First Edition). Springer, Berlin, 2007: p. 388. https://doi.org/10.1007/978-3-540-34591-6
17. **Mai, B.D.** Analyzing Frequency Spectra of Dielectric Loss to Clarify Influence of L,α-alanine Doping on Phase Transition in Triglycine Sulfate *Materials Science (Medžiagotyra)* (Early Access). https://doi.org/10.5755/j02.ms.29313
18. **Galiyarova, N.M.** Critical Slowing Down of Relaxing Domain Walls and Interfaces in Phase Transition Vicinities *Ferroelectrics* 170 (1) 1995: pp. 111 – 121. https://doi.org/10.1080/00150199508014197
19. **Yurtseven, H., Kiraci, A.** Temperature Dependence of the Polarization and the Dielectric Constant Near the Paraelectric-Ferroelectric Transitions in $BaTiO_3$ *Journal of Molecular Modeling* 19 2013: pp. 3925 – 3930. https://doi.org/10.1007/s00894-013-1927-4
20. **Podgorny, Y., Sigov, A., Vorotilov, K.** Once Again on the Hysteresis Loop: Leakage Current Consideration *Ferroelectrics* 573 (1) 2021: pp. 1 – 8. https://doi.org/10.1080/00150193.2021.1890459
21. **Thangavel, V., Farsa, R., Balu, P., Kadhiravan, S., Ramamoorthy, B.** All-Organic Composites of Ferro- and Piezoelectric Phosphonium Salts for Mechanical Energy Harvesting Application *Chemistry of Materials* 31 (15) 2019: pp. 5964 – 5972. https://doi.org/10.1021/acs.chemmater.9b02409